Research Article | Vol. 30, No. 19 / 12 Sep 2022 / Optics Express 34411

Optics EXPRESS

Repetition frequency tunability and stability of BH InAs/InP QD and InGaAsP/InP QW two-section mode-locked laser diodes

VLADYSLAV CHERNIAK,[1,*] MARLENE ZANDER,[2] MARTIN MOEHRLE,[3] WOLFGANG REHBEIN,[3] AND JAN C. BALZER[1]

[1] *University of Duisburg-Essen, Bismarckstr. 81, 47057 Duisburg, Germany*
[2] *Infineon Technologies Dresden, Development Center ATV HP, Dresden 01099, Germany*
[3] *Fraunhofer Heinrich-Hertz-Institut, Berlin 10587, Germany*
[*] *vladyslav.cherniak@uni-due.de*

Abstract: Ultra-high repetition rate (UHRR) mode-locked laser diodes (MLLD) have shown promising results for applications based on optical sampling such as asynchronous optical sampling (ASOPS), optical sampling by repetition-rate tuning (OSBERT), and optical ranging. Important metrics to consider are the repetition frequency (RF) and the RF linewidth. Here, we compare two monolithically integrated MLLDs. A quantum dot (QD) MLLD with an RF of approx. 50.1 GHz and a quantum well (QW) MLLD with an RF of approx. 51.4 GHz. The tunability of the RF is characterized by sweeping the lasers pump current, temperature, and saturable absorber (SA) reverse voltage. The QW MLLD has a tuning range of 31 MHz with an average RF linewidth of 53 kHz, while the QD MLLD has a smaller tuning range of 26 MHz with a higher average RF linewidth of 172 kHz.

1. Introduction

Ultrafast spectroscopy such as optical pump probe and optical sampling enabled scientists to observe ultrafast phenomena [1]. Many state of the art measurement techniques such as terahertz time-domain spectroscopy (THz-TDS) and optical ranging are based on optical pump probe or optical sampling [2–4]. A shared characteristic of the techniques is the use of pulsed light sources. From the first driving sources, which were dye lasers, researchers have developed a variety of laser systems, such as titanium-sapphire lasers and ultrafast fiber lasers, which have enabled breakthroughs for optical sampling based applications like THz-TDS [5–7]. However, these lasers still make up a large part of system cost and size [8]. To overcome this issue, new, compact, and inexpensive light sources based on monolithic edge-emitting semiconductor laser diodes have been investigated for terahertz generation in recent years [9,10]. Even commercially available laser diodes have been successfully used as light sources for terahertz systems [11]. In previous work, we have shown that compact and modular systems can be realized with such light sources [12]. As an example for optical ranging, P. Trocha et al. presented ultra-fast optical ranging with scanning rates of 500 MHz based on a quantum-dash mode-locked lasers [13].

The fundamental principle of all optical sampling and pump probe based measurement techniques incorporates a variable time delay between the transmitting or receiving arm of the optical system. Typical examples for the realization of the optical delay are mechanically controlled optical delay units (ODU) or electronically controlled Mach-Zehnder-modulators. These methods have the downside of additionally added uncertainties, cost, and complexity. Rehn et al. have analyzed the the effect of sampling errors caused by ODUs [14]. Other methods exploit a difference of the repetition frequency (RF) of two mode-locked lasers. This method is called asynchronous optical sampling (ASOPS) or dual comb spectroscopy (DCS) [3]. A similar effect can be achieved by tuning the RF of a single mode-locked laser. There exist three different

#468031 https://doi.org/10.1364/OE.468031
Journal © 2022 Received 15 Jun 2022; revised 22 Jul 2022; accepted 22 Aug 2022; published 6 Sep 2022

methods: (i) optical sampling by repetition frequency modulation (OSREFM) [15], (ii) optical sampling by cavity tuning (OSCAT) [16], and (iii) optical sampling by electronic repetition-rate tuning (OSBERT) [17], which has been shown by Bajek et al. achieve megahertz scan rates [18]. For OSBERT, the scanning range is calculated as a function of RF and introduced fiber length difference [17]:

$$\Delta\tau = \frac{l \cdot n \cdot f}{c} \left(\frac{1}{f} - \frac{1}{f + \Delta f}\right), \quad (1)$$

where, l the fiber length difference, n the refractive index of the fiber, c the speed of light, f the RF, and Δf the maximum tuning range of the RF. ASOPS, OSCAT, and OSBERT show, that without an intentionally introduced optical delay, sampling can be realized. Hence, the RF and the RF linewidth, i.e. the tunability and stability of the laser, has an impact on the measurement results comparable to the uncertainties of ODUs [19]. A formula for calculating the introduced jitter was presented by Kefelian et al. [20]:

$$\sigma_{pp}(N) = \frac{1}{f}\sqrt{\frac{\Delta\nu N}{2\pi f}}, \quad (2)$$

where $N = n \cdot l \cdot f / c$ and $\Delta\nu$ is the RF linewidth. For this reason, we are investigating two laser diodes: a two-section buried heterostructure (BH) quantum dot laser diode (QD) and a quantum well laser diode (QW) processed from the same mask, with a total length of 840 µm including an absorber with the length of 50 [21,22]. A detailed schematic and explanation of the devices is provided by Ding et al in [23]. The mode locking is ensured by reverse biasing of the saturable absorber (SA) section. Both lasers are research grade state of the art MLLDs and have shown to be promising light sources for future terahertz systems [24]. A study on the group velocity dispersion can be found in Ref. [23].

The paper is structured as follows. First, we describe the measurement setup. Then we present and discuss the measurements. We analyze the change in RF of both MLLDs by changing laser temperature and pump current. For operation points with a narrow RF linewidth, we perform RF tuning by varying the reverse bias at the MLLDs SA.

2. Experimental setup

The simplified block diagram of the setup is depicted in Fig. 1. A laser controller (LC, Thorlabs Pro800) is used for setting the pump current and temperature of the laser. In addition, a source measure unit (SMU, Keysight b2901a) is used to supply the SA with a well-defined bias voltage, while limiting the absorber current to 30 mA to prevent damage to the laser. An erbium-doped fiber amplifier (EDFA, Thorlabs EDFA100P) boosts the optical power at the photodiode (PD, u^{2}t photonics XPDV2020R) to 5 mW which is the highest allowed optical power input. The PD converts the optical signal into an electrical signal that is measured by an electrical spectrum analyzer (ESA, Anritsu MS2760A). One percent of the amplified optical power is fed into an optical spectrum analyzer (OSA, Anritsu MS9740A).

The MLLDs are characterized by sweeping the pump current and temperature. The pump current is swept from 200 mA to 400 mA in 1 mA step. During a sweep, a fixed temperature is set between 9 °C and 30 °C which in increased by 0.2 °C steps. The SA voltage is set to 0 V during the temperature and current sweeps. For each combination of current and temperature, an electrical spectrum is measured. Later, a sweep of the SA voltage is performed from 0 V to -1.4 V in 2 mV steps, at temperature and pump current combination chosen by RF linewidths obtained from the previous measurements. The data acquisition is realized as follows. First, a parameter combination of the pump current and the laser temperature is set. Then, a 20 s pause takes place to give the laser time to settle to a stable working point. The OSA is set to a measurement window ranging from 1535 nm to 1585 nm with a resolution of 0.2 nm. A single measurement is

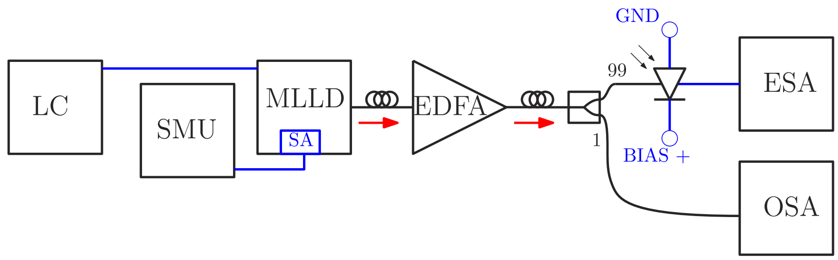

Fig. 1. Schematic of the experimental setup. Electrical connections are shown in blue and optical fiber connections in black. Red arrows are indicating the direction of laser light emission.

triggered after the pause. Next, the electrical spectrum is measured by taking 100 averages. A window size of 10 MHz and a resolution of 1 kHz is used. To avoid damage and degradation of the laser modules, we have not covered the entire range of parameter combinations such as higher temperatures. We have skipped values below 200 mA since the MLLDs become unstable and the output power is low.

3. Experimental results

3.1. Temperature and pump current tuning

Figure 2 depicts the overall trends of RF tunability over the measured parameter space. Fig. 2(a) and 2(c) depict the results for the QD and Fig. 2(b) and 2(d) depict the results for the QW laser. All shown figures are plotted relative to the lowest accruing frequency in the data set. A distinct difference in their behavior is the confined RF of the QD over the parameter space. The maximum change in RF is approx. 54 MHz. At pump currents around 300 mA a change in temperature has a small impact (20 MHz) on the RF. Overall, no clear trend can be seen across temperature and pump current. In contrast, an increase in RF for higher currents and temperatures can be seen for the QW laser. A maximum tunability of approx. 108 MHz is achieved. Fig. 2(c) and 2(d) depict the change in RF with increasing temperature and pump current. The RF increases with temperature and pump current in case of the QW. The QD has its highest RF values at lower temperatures and pump currents, following a random, confined trend over the parameter space. In summary, the QD laser shows a higher temperature invariance while the RF of the QW laser can be detuned over a larger range.

Figure 3 illustrates the RF stability for each combination of temperature and current. The RF linewidth is calculated from the electrical spectra as the -3 dB linewidth and is color coded. To increase the contrast of the colormaps, the color bar is limited to 600 kHz. Overall, the RF linewidth of the QD, as depicted in Fig. 3(a), shows a mean RF linewidth of 371 kHz with a standard deviation of 511 kHz over the complete parameter space compared to the QWs a mean RF linewidth of 153 kHz with a standard deviation of 360 kHz, as shown in Fig. 3(b). The lowest measured RF linewidths for the QD and QW devices are 17 kHz and 10 kHz, respectively. Explicitly, the literature shows comparison between QW and QD devices, where QD devices outperform QW devices [25]. Examples for QW devices with RF linewidths as low as 30 kHz [26] and RF linewidths as low as 1.6 kHz for QD devices [20] are shown. However, most of these investigations compare single operation points giving the best and most stable results for the investigated devices. In this study, we focus on the tuning aspect and show that the average RF linewidth of the QW device over the investigated parameter range is lower.

The results are in good agreement with MLLD theory as presented by Grillot et al. [27] and the measurement results shown by Zander et al. [21]. The restricted RF of the QD laser is a characteristic feature of the high-quality mode locking expected from QD laser diodes. However,

Optics EXPRESS

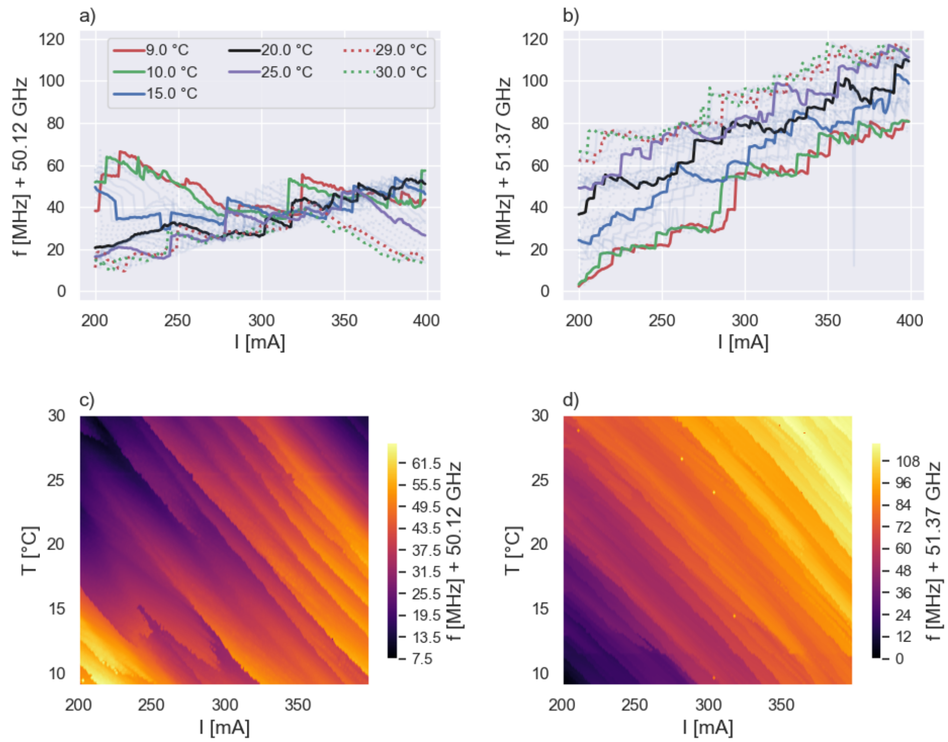

Fig. 2. Change of RF over pump current with increasing temperature of (a) the QD laser and (b) the QW. Certain temperatures are highlighted by contrast, indicating the overall trend. The change of the central RF represented in a colormap over all measured working points for the QD (c) and the QW (d) laser.

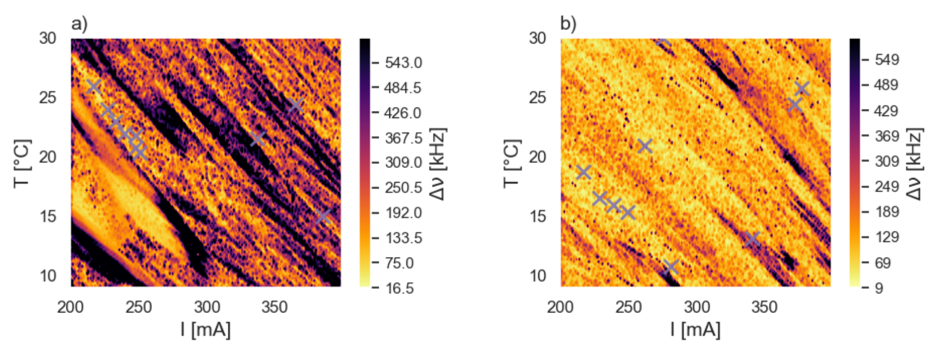

Fig. 3. RF linewidth of (a) the QD laser and (b) the QW laser. The RF linewidth is evaluated after a wait time 20 s, measured in the electrical spectrum with an averaging of 100. 10 points of operation are marked by crosses and used in 3.2 for investigation on RF tunability utilizing the SA.

for application based on OSBERT and ASOPS this feature is not desirable, since it limits the applicable detection range. On top of that, the QW used in this study is superior in terms of RF linewidth over a broad parameter space. This illustrates that sweeping statements about QD and QW structures should be taken with caution. It always depends on the respective application and the degree of optimization of the active material. With a minimum RF linewidth of 10 kHz, the results of the QW laser are comparable with state-of-the-art QDash lasers without external feedback [28]. For further analysis regarding the tunability of the RF by the SA voltage, we identified 10 operating points with particularly low RF linewidth for both lasers. These 10 points are marked by crosses in Fig. 3 and are used in the following subsection.

3.2. Saturable absorber tuning

We evaluate the change of RF over the applied SA reverse voltage in steps of 2 mV and measure the RF linewidth at each point. Fig. 4 illustrates an exemplarily chosen operation point for both devices. Both, the QD and the QW show a steady and almost linear change in RF starting from 0 V reverse voltage up to a certain voltage. These regions are shaded green for both figures. For both MLLDs, a current limit of 30 mA was set. The SMU limits the applied voltage as soon as the compliance current is reached. Hence, depending on the point of operation after a certain applied reverse voltage, no change in RF is measured. The QD never reaches the compliance during the experiments. However, a change in RF still stops after a certain applied reverse voltage. It is noted that the slope of the RF changes is inverse to each other for both devices. The range of achievable tunability is on average slightly higher for the QW device and highly dependent on the point of operation. The RF linewidth is very stable for most points of operation for the QW over the whole tuning range, while the QD shows a very unstable and rapidly changing RF linewidth, even within the tuning range of linear change of RF.

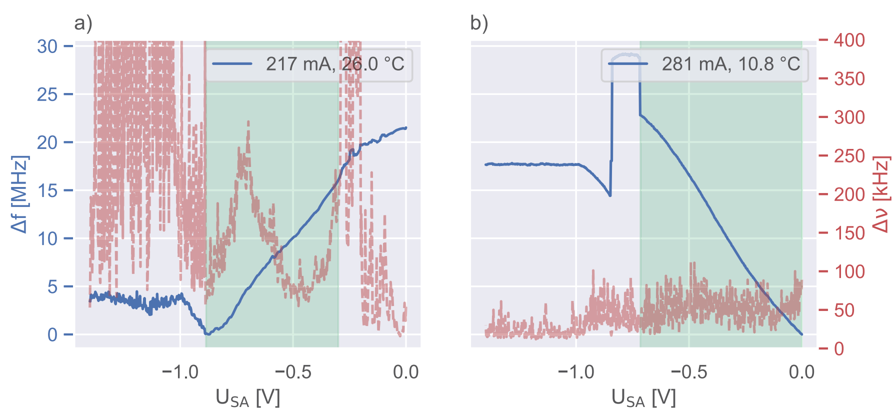

Fig. 4. (a) RF and RF linewidth of the QD laser with varying SA reverse bias. (b) RF and RF linewidth of the QW laser with changing SA reverse bias. Region of continuous and stable tuning is shadowed green.

Comparing the RF linewidths shown in Fig. 4(a) and 4(b) illustrates why the QW is more advantageous than the QD in this context. The QDs lowest RF linewidth (10 kHz) outperforms the lowest QW linewidth (17 kHz) at certain values of the applied reverse voltage. However, the further the reverse bias deviates from these optimized conditions the higher the RF linewidth. But in the case of the QW, the RF can be detuned over a wide range without significantly changing the RF linewidth gets. On the other hand, the QD laser generally has a lower dependence on temperature and injection current on the RF (cf. Fig. 2), especially for 300 mA. This is a major advantage of QD lasers which is given by the 0-D structure of the gain material. However, this is disadvantageous in terms of tunability.

The ten operating points which were previously selected are depicted in Table 1. In terms of application, the listed results can be used to calculate the scan range and timing jitter from Eqs. (1) and (2). With the QD 5 operation point at 217 mA and 26 °C, a scan range of 91.89 ps and a timing jitter of 744.1 fs can be achieved, assuming a 10 m long standard optical fiber. With the QW 6 point of operation at 281 mA and 10.8 °C, a scan range of 22.197 ps and a timing jitter of 405.2 fs can be achieved with an equal set up.

Table 1. Points of operation for the QW and QD extracted over a linear tunable range

Label	Max. Δf [MHz]	Mean $\Delta\nu$ [kHz]	Std. dev. $\Delta\nu$ [kHz]	Label	Max. Δf [MHz]	Mean $\Delta\nu$ [kHz]	Std. dev. $\Delta\nu$ [kHz]
QW 0	30.6	58.6	21.9	QD 0	24.6	294.7	290.4
QW 1	31.4	68	21	QD 1	17.7	200.5	230.1
QW 2	26.3	56.3	22.1	QD 2	19.5	312.9	491.8
QW 3	11	55.2	16.1	QD 3	26.3	336.1	255.3
QW 4	26.1	56.7	21.4	QD 4	15.2	263.7	250.8
QW 5	28.8	53	20.4	QD 5	19.7	172.9	128.6
QW 6	22.5	53.7	17.8	QD 6	16.4	193.5	118.6
QW 7	23.1	60	22.5	QD 7	17.1	345	266.8
QW 8	26.6	54.2	21.5	QD 8	16.8	557.9	837.1
QW 9	24.8	61.8	21.2	QD 9	16.4	268.5	359.6

Comparing the experimental results with the theoretical analysis performed by Ejidike et al, we can make an estimation for the usability of our devices in terms of application and performance [29]. The QW laser provides comparable jitter to the theoretical analysis, showing its usefulness for the application discussed. The QD laser has a higher average jitter. Compared to the QD laser, this means that averaging is required to achieve similar performance. In addition, Fig. 4 shows a low jitter over the tuning range for the QW laser, while the QD laser has a large fluctuation over the tuning range. Therefore, in the case of the QD laser, reverse bias dependent jitter results in inconsistent timing jitter within a time trace.

Figure 5 depicts the evolution of the optical spectra as a function of the SA voltage for Fig. 5(a) the QD and for 5(b) the QW. The chosen parameters are equal to those represented in Fig. 4. The change of the geometric central wavelength Δλ relative to the lowest measured central wavelength as well as the optical 10 dB bandwidth $\Delta\lambda_{10dB}$ is presented in Fig. 5(c) for the QD and 5(d) for the QW. The green shaded background indicates the range of linear and stable tuning conditions as shown in Fig. 4.

Both, the higher tuning range difference as well as the direction of change are equal to the differences shown in Fig. 5. This indicates that the main cause can be contributed to an overall change in optical length of the cavity. This can be attributed to joule heating induced cavity length variations, changes in refractive index which can be caused by the Pockels' effect [30], or the quantum-confined Stark effect [31,32]. The different directions of change indicate different dominant effects within the QW and QD structures.

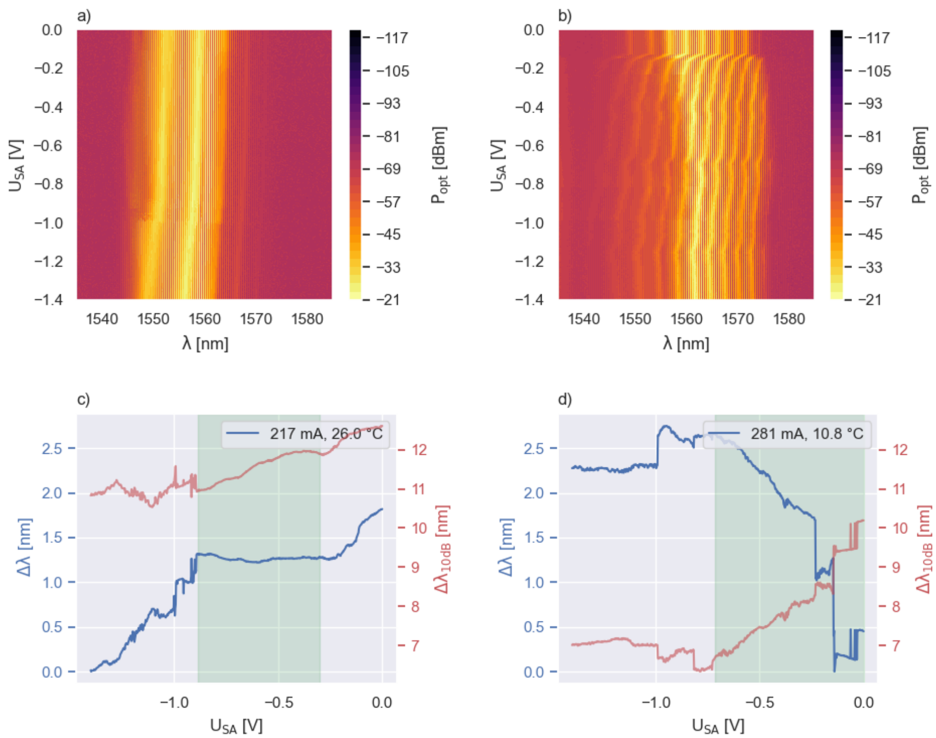

Fig. 5. Evolution of the optical spectra as a function of the SA voltage for (a) the QD and (b) the QW. As well the change of the relative central operation wavelength and optical 10 dB bandwidth over the applied SA voltage for (c) the QD and (d) the QW. The region of continuous and stable tuning is shaded in green.

4. Conclusion

In this work, we compared two MLLDs, a QD and a QW, from an equal processing node in term of RF tunability and stability by measuring electrical spectra over a large parameter set. We show that contrary to previous publications that the QW achieves better performance and stability compared to its QD counterpart. The achievable tuning range for the QW device is higher and the RF linewidth is stable over a substantial portion of the observed points of operation. Overall, we show that the QW device in this study is a superior choice for applications based on RF change and stability like OSBERT and ASOPS, compared to an equally processed QD. However, due to the small sample size of two devices further investigation in the tuneability and stability of RF across different monolithically integrated laser sources should be conducted.

Funding. Mercur Mercator Research Center Ruhr (Pr-2019-0009).

Acknowledgments. We acknowledge support by the Open Access Publication Fund of the University of Duisburg-Essen. This work has been supported by the Mercur Mercator Research Center Ruhr.

Disclosures. The authors declare no conflicts of interest.

Data Availability. Data underlying the results presented in this paper are not publicly available at this time but may be obtained from the authors upon reasonable request.

References

1. D. H. Auston, A. M. Johnson, P. R. Smith, and J. C. Bean, "Picosecond optoelectronic detection, sampling, and correlation measurements in amorphous semiconductors," Appl. Phys. Lett. **37**(4), 371–373 (1980)..

Optics EXPRESS

2. M. Van Exter, C. Fattinger, and D. Grischkowsky, "Terahertz time-domain spectroscopy of water vapor," Opt. Lett. **14**(20), 1128–1130 (1989).
3. P. A. Elzinga, F. E. Lytle, Y. Jian, G. B. King, and N. M. Laurendeau, "Pump/Probe Spectroscopy By Asynchronous Optical Sampling," Appl. Spectrosc. **41**(1), 2–4 (1987).
4. Z. Zhu and G. Wu, "Dual-Comb Ranging," Engineering **4**(6), 772–778 (2018).
5. P. Shumyatsky and R. R. Alfano, "Terahertz sources," J. Biomed. Opt. **16**(3), 033001 (2011).
6. B. Sartorius, H. Roehle, H. Künzel, J. Böttcher, M. Schlak, D. Stanze, H. Venghaus, and M. Schell, "All-fiber terahertz time-domain spectrometer operating at 1.5 µm telecom wavelengths," Opt. Express **16**(13), 9565–9570 (2008).
7. M. Naftaly, N. Vieweg, and A. Deninger, "Industrial applications of terahertz sensing: State of play," Sensors **19**(19), 4203 (2019).
8. T. Hochrein, ""Markets, Availability, Notice, and Technical Performance of Terahertz Systems: Historic Development, Present, and Trends," J. Infrared, Millimeter Terahertz Waves **36**(3), 235–254 (2015).
9. H. Elayan, O. Amin, B. Shihada, R. M. Shubair, and M. Alouini, "Terahertz Band : The Last Piece of RF," IEEE Open J. Commun. Soc. **1**, 1–32 (2020).
10. D. Molter, M. Kolano, and G. von Freymann, "Terahertz cross-correlation spectroscopy driven by incoherent light from a superluminescent diode," Opt. Express **27**(9), 12659 (2019).
11. K. H. Tybussek, K. Kolpatzeck, F. Faridi, S. Preu, and J. C. Balzer, "Terahertz time-domain spectroscopy based on commercially available 1550 nm Fabry-Perot laser diode and ErAs:In(Al)GaAs photoconductors," Appl. Sci. **9**(13), 2704 (2019).
12. V. Cherniak, K. Kolpatzeck, X. Liu, K. Tybussek, D. Damyanov, T. Schultze, A. Czylwik, and J. C. Balzer, "Compact and Inexpensive Terahertz System Driven by Monolithically Integrated Commercial Light Sources," *Int. Conf. Infrared, Millimeter, Terahertz Waves, IRMMW-THz* **2021-Augus**, 2021–2022 (2021).
13. P. Trocha, J. N. Kemal, Q. Gaimard, G. Aubin, F. Lelarge, A. Ramdane, W. Freude, S. Randel, and C. Koos, "Ultra-fast optical ranging using quantum-dash mode-locked laser diodes," Sci. Rep. **12**(1), 1–12 (2022).
14. A. Rehn, D. Jahn, J. C. Balzer, and M. Koch, "Periodic sampling errors in terahertz time-domain measurements," Opt. Express **25**(6), 6712 (2017).
15. T. Furuya, E. S. Estacio, K. Horita, C. T. Que, K. Yamamoto, F. Miyamaru, S. Nishizawa, and M. Tani, "Fast-scan terahertz time domain spectrometer based on laser repetition frequency modulation," Jpn. J. Appl. Phys. **52**(2R), 022401 (2013).
16. R. Wilk, T. Hochrein, M. Koch, M. Mei, and R. Holzwarth, "Terahertz spectrometer operation by laser repetition frequency tuning," J. Opt. Soc. Am. B **28**(4), 592 (2011).
17. D. Bajek and M. A. Cataluna, "Fast optical sampling by electronic repetition-rate tuning using a single mode-locked laser diode," Opt. Express **29**(5), 6890 (2021).
18. D. Bajek and M. A. Cataluna, "Megahertz scan rates enabled by optical sampling by repetition-rate tuning," Sci. Rep. **11**(1), 22995 (2021).
19. D. Jahn, S. Lippert, M. Bisi, L. Oberto, J. C. Balzer, and M. Koch, "On the Influence of Delay Line Uncertainty in THz Time-Domain Spectroscopy," J. Infrared, Millimeter, Terahertz Waves **37**(6), 605–613 (2016).
20. F. Kéfélian, S. O'Donoghue, M. T. Todaro, J. G. McInerney, and G. Huyet, "RF linewidth in monolithic passively mode-locked semiconductor laser," IEEE Photonics Technol. Lett. **20**(16), 1405–1407 (2008).
21. M. Zander, W. Rehbein, M. Moehrle, S. Breuer, D. Franke, M. Schell, K. Kolpatzeck, and J. C. Balzer, "High performance BH InAs/InP QD and InGaAsP/InP QW mode-locked lasers as comb and pulse sources," in *Optical Fiber Communication Conference (OFC) 2020* (OSA, 2020), p. T3C.4.
22. M. Zander, W. Rehbein, M. Mohrle, S. Breuer, D. Franke, and D. Bimberg, "InAs/InP QD and InGaAsP/InP QW comb lasers for 1 Tb/s transmission," in *2019 Compound Semiconductor Week (CSW)* (IEEE, 2019), pp. 1.
23. Y. Ding, W. Rehbein, M. Moehrle, M. Zander, M. Schell, K. Kolpatzeck, and J. C. Balzer, "Group velocity dispersion in high-performance BH InAs/InP QD and InGaAsP/InP QW two-section passively mode-locked lasers," Opt. Express **30**(14), 24353 (2022).
24. K. Kolpatzeck, X. Liu, K.-H. Tybussek, L. Häring, M. Zander, W. Rehbein, M. Moehrle, A. Czylwik, and J. C. Balzer, "System-theoretical modeling of terahertz time-domain spectroscopy with ultra-high repetition rate mode-locked lasers," Opt. Express **28**(11), 16935 (2020).
25. M. G. Thompson, A. R. Rae, M. Xia, R. V Penty, and I. H. White, "InGaAs Quantum-Dot Mode-Locked Laser Diodes," Appl. Sci. **15**(3), 661–672 (2009).
26. K. Merghem, A. Akrout, A. Martinez, G. Moreau, J.-P. Tourrenc, F. Lelarge, F. Van Dijk, G.-H. Duan, G. Aubin, and A. Ramdane, "Short pulse generation using a passively mode locked single InGaAsP/InP quantum well laser," Opt. Express **16**(14), 10675 (2008).
27. W. W. Chow, B. Dong, S. Ding, H. Huang, and J. Bowers, "Multimode Physics in the Mode Locking of Semiconductor Quantum Dot Lasers," Appl. Sci. **12**(7), 3504 (2022).
28. J. N. Kemal, P. Marin-Palomo, K. Merghem, G. Aubin, F. Lelarge, A. Ramdane, S. Randel, W. Freude, and C. Koos, "32QAM WDM transmission at 12 Tbit/s using a quantum-dash mode-locked laser diode (QD-MLLD) with external-cavity feedback," Opt. Express **28**(16), 23594 (2020).
29. I. Ejidike, R. A. McCracken, and D. Bajek, "Modelling two-laser asynchronous optical sampling using a single 2-section semiconductor mode-locked laser diode," Opt. Express **30**(3), 3289 (2022).

Optics EXPRESS

30. S. Arahira and Y. Ogawa, "Repetition-frequency tuning of monolithic passively mode-locked semiconductor lasers with integrated extended cavities," IEEE J. Quantum Electron. **33**(2), 255–264 (1997).
31. J. S. Weiner, D. A. B. Miller, and D. S. Chemla, "Quadratic electro-optic effect due to the quantum-confined Stark effect in quantum wells," Appl. Phys. Lett. **50**(13), 842–844 (1987).
32. Y. H. Kuo, Y. K. Lee, Y. Ge, S. Ren, J. E. Roth, T. I. Kamins, D. A. B. Miller, and J. S. Harris, "Strong quantum-confined Stark effect in germanium quantum-well structures on silicon," Nature **437**(7063), 1334–1336 (2005).

DOI: 10.1364/OE.468031
URN: urn:nbn:de:hbz:465-20220923-140233-8